Paleoceanography and Paleoclimatology

RESEARCH ARTICLE
10.1029/2021PA004233

Natural and Anthropogenic Forcing of Multi-Decadal to Centennial Scale Variability of Sea Surface Temperature in the South China Sea

Nathalie F. Goodkin[1,2,3], Dhrubajyoti Samanta[2,3], Annette Bolton[2,3,4], Maria Rosabelle Ong[1,2,5], Phan Kim Hoang[6], Si Tuan Vo[6], Kristopher B. Karnauskas[7,8], and Konrad A. Hughen[9]

[1]Department of Earth and Planetary Sciences, American Museum of Natural History, New York, NY, USA, [2]Asian School of the Environment, Nanyang Technological University, Singapore, Singapore, [3]Earth Observatory of Singapore, Nanyang Technological University, Singapore, Singapore, [4]Now at: Institute for Environmental Science & Research, Christchurch, New Zealand, [5]Lamont Doherty Earth Observatory, Columbia University, Palisades, NY, USA, [6]Institute of Oceanography, Vietnam Academy of Science and Technology, Hà Nội, Vietnam, [7]Department of Atmospheric and Oceanic Sciences, University of Colorado Boulder, Boulder, CO, USA, [8]Cooperative Institute for Research in Environmental Sciences, University of Colorado Boulder, Boulder, CO, USA, [9]Marine Chemistry and Geochemistry, Woods Hole Oceanographic Institution, Woods Hole, MA, USA

Abstract Four hundred years of reconstructed sea surface temperatures (SSTs) from a coral located off the coast of Vietnam show significant multi-decadal to centennial-scale variability in wet and dry seasons. Wet and dry season SST co-vary significantly at multi-decadal timescales, and the Interdecadal Pacific Oscillation (IPO) explains the majority of variability in both seasons. A newly reconstructed wet season IPO index was compared to other IPO reconstructions, showing significant long-term agreement with varying amplitude of negative IPO signals based on geographic location. Dry season SST also correlates to sea level pressure anomalies and the East Asian Winter Monsoon, although with an inverse relationship from established interannual behavior, as previously seen with an ocean circulation proxy from the same coral. Centennial-scale variability in wet and dry season SST shows 300 years of near simultaneous changes, with an abrupt decoupling of the records around 1900, after which the dry season continues a long-term cooling trend while the wet season remains almost constant. Climate model simulations indicate greenhouse gases as the largest contributor to the decoupling of the wet and dry season SSTs and demonstrate increased heat advection to the western South China Sea in the wet season, potentially disrupting the covariance in seasonal SST.

Dhrubajyoti Samanta and Annette Bolton contributed equally to this work.

Key Points:

- South China Sea wet season sea surface temperature (SST) reflects the Interdecadal Pacific Oscillation (IPO) on decadal timescales and indicate changes in the IPO spatial pattern with time
- Dry season SST is influenced by both the IPO and winter East Asian Monsoon on decadal timescales
- Wet and dry season SSTs show consistent centennial variability from 1600 until 1900 when they uncouple due to greenhouse gas forcing

Supporting Information:

Supporting Information may be found in the online version of this article.

Correspondence to:

N. F. Goodkin,
ngoodkin@amnh.org

Citation:

Goodkin, N. F., Samanta, D., Bolton, A., Ong, M. R., Hoang, P. K., Vo, S. T., et al. (2021). Natural and anthropogenic forcing of multi-decadal to centennial scale variability of sea surface temperature in the South China Sea. *Paleoceanography and Paleoclimatology*, *36*, e2021PA004233. https://doi.org/10.1029/2021PA004233

Received 26 JAN 2021
Accepted 15 SEP 2021

1. Introduction

Limited instrumental records of sea surface temperature (SST) have hindered our ability to fully understand the natural long-term climate variability driven by surface ocean-atmosphere interactions, particularly in Southeast and East Asia where approximately 30% of the world's population resides (Morton & Blackmore, 2001; United Nations, 2019). Recent modeling studies have begun to document the uncertainty in the centennial-scale behavior of SST in the Western Pacific Ocean and surrounding seas, further emphasizing our need to reconstruct ocean hydrography at a high temporal resolution over longer periods (Karnauskas et al., 2012; Samanta et al., 2018).

Complicating our understanding of climate in the marginal seas of the Maritime Continent are the changing interactions between climate drivers of surrounding areas. Climate drivers in Southeast Asia and the marginal seas, including the South China Sea (SCS), are complex and operate at multiple frequencies. For example, the East Asian Monsoon (EAM) varies primarily on a seasonal timescale, whereas the El Niño Southern Oscillation (ENSO) and the Interdecadal Pacific Oscillation (IPO) exert influence on interannual to interdecadal timescales, respectively. The EAM is defined by seasonal shifts in winds and moisture delivery to East Asia from the Indian and Pacific Oceans. In the summer, winds blow from the Indian Ocean over the SCS onto the Asian continent, driving precipitation. In the winter, winds reverse, delivering cold, dry air from the Pacific Ocean across the East Asian continent to the SCS. These winds have a significant impact, driving seasonal changes in ocean circulation, temperature and precipitation (Lau & Li, 1984; B.

Wang et al., 2000), with strong low-frequency changes resulting from interactions with other climate systems (Goodkin et al., 2019; Hu et al., 2000; Xu et al., 2006). However, the EAM is not the sole influence on regional climate in the SCS and there are substantial impacts from ENSO (e.g., D'Arrigo, Jacoby, et al., 2005; Xie et al., 2009) and Pacific and Indian ocean SSTs (Li et al., 2010; Samanta et al., 2020; Wu et al., 2009). ENSO is a coupled atmosphere-ocean mode of tropical climate variability, generally defined by SST anomalies in the equatorial Pacific, that modulates changes to global weather patterns via teleconnections (Klein et al., 1999; Lau, 1997). The IPO is a mode of interdecadal variability in the Pacific, based on the difference between SST anomalies averaged over the central equatorial and combined northwest and southwest Pacific regions (Power et al., 1999; Salinger et al., 2001). Temperatures in the Western Pacific Warm Pool (WPWP) and the tropical Pacific Ocean, in general, are known to influence climate regionally to globally, and subsequently impact the behavior of ENSO and the IPO (Abram et al., 2009; Cravatte et al., 2009; D'Arrigo, Wilson, & Jacoby, 2006; Webster & Lukas, 1992; Yan et al., 1992). On decadal time scales, SST anomalies in the Pacific Ocean change locations between equatorial and temperate regions—a "footprint" statistically described by the IPO. In turn, the IPO impacts the size and temperature of the WPWP and influences the behavior of ENSO (Crueger et al., 2009; D'Arrigo, Jacoby, et al., 2005; D'Arrigo & Ummenhofer, 2015). How all these climate drivers come together to impact the SCS is still a matter of ongoing study. However, the IPO is known to impact the EAM directly as well as through its impact on ENSO, making it challenging to deconvolve teleconnections in the region (Li & Yang, 2010; Song & Zhou, 2014, 2015; L. Wang et al., 2008). Some coupled climate models show strong, anti-phase, centennial SST changes linking the warm pool and the western boundary of the SCS along the Vietnam coast, but both instrumental and paleorecords are too short and sparse to validate this relationship (Karnauskas et al., 2012).

Extending paleoclimate records in the SCS to capture centennial-scale variability allows for an investigation of behavior beyond the limit of regional instrumental records, including the Little Ice Age (LIA). The LIA is the most recent example of natural, centennial-scale changes to hemispheric temperature occurring in the last couple of millennia (Bradley & Jones, 1993; Dunbar & Cole, 1999). Characterized by a 1°–2°C depression of northern hemisphere surface temperatures, the LIA lasted from the 1300s into the 1880s. The LIA led to harsh winters in the Eastern United States and Europe, and significant disruptions to the hydrologic cycle across Asia where severe and prolonged droughts became more common (Buckley et al., 2014; Mann et al., 1999; Moberg et al., 2006). Significant evidence also exists for LIA-affiliated cooling in the tropics (DeLong et al., 2012, 2013; Deng et al., 2017; Newton et al., 2006; Watanabe et al., 2001), and shifts in hydrologic patterns hypothesized to result from the contraction of the inter-tropical convergence zone (Griffiths et al., 2016; H. Yan et al., 2015).

Massive corals provide unique reservoirs for paleoclimate reconstructions because they allow for monthly to sub-monthly climate reconstruction of SST at one location (Beck et al., 1992; D. Chen et al., 2020; Smith et al., 1979). In addition, corals can grow continuously for several centuries, recording the ambient seawater conditions indicative of surface climate including SST, sea surface salinity, pollutants, and nutrient availability, amongst others (Alibert & McCulloch, 1997; de Villiers et al., 1994; Gagan et al., 2002; Goodkin et al., 2015; Ren et al., 2017; B. S. Wang et al., 2011). One critical tool for paleoclimate reconstructions is the inverse relationship between SST and the concentration of strontium (Sr) relative to calcium (Ca) in the coral skeleton (Beck et al., 1992; Smith et al., 1979; Weber, 1973), which has been used successfully to reconstruct SST at seasonal-to-multidecadal frequencies from corals around the world (e.g., Carilli et al., 2014; Cole et al., 1993; DeLong et al., 2014; Goodkin et al., 2008; Hughen et al., 1999; Kilbourne et al., 2010; Ramos et al., 2020).

Regional reconstructions of Southeast Asian climate are mostly terrestrial based, focusing on tree rings and speleothems, and tend to be biased toward summer signals (D'Arrigo, Jacoby et al., 2005; D'Arrigo, Wilson, Deser, et al., 2005; J. Liu et al., 2015). Several valuable coral proxy records exist from the SCS, but are either too short to fully examine centennial variability (Deng et al., 2013; Mitsuguchi et al., 2008; Song et al., 2012), or are limited to discontinuous narrow windows further back in time (Deng et al., 2017; C. C. Liu et al., 2019). Here we present the first continuous, multi-century, seasonal SST record from the SCS, and use it to examine decadal and centennial-scale variability over the past 400 years.

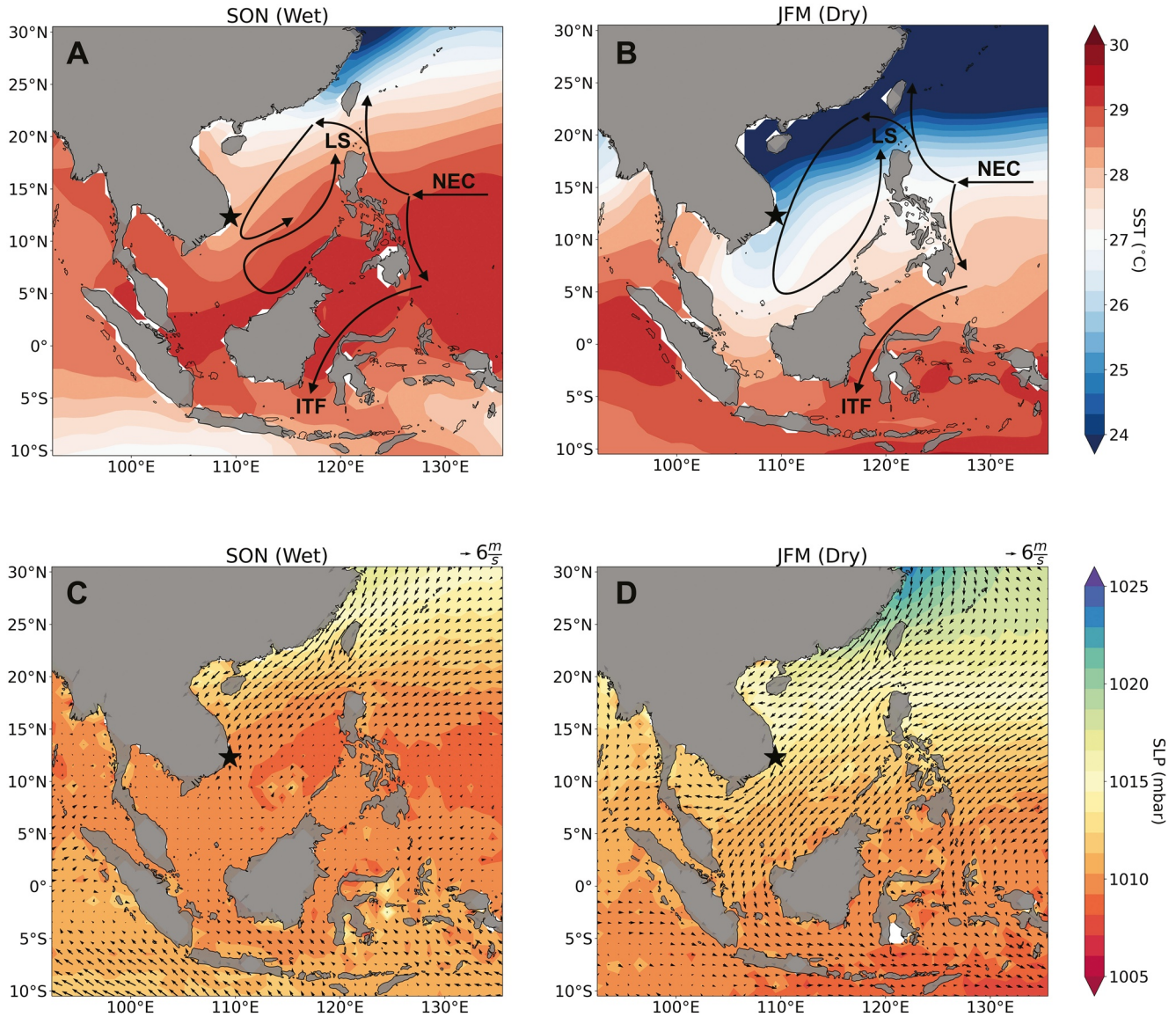

Figure 1. South China Sea (SCS) seasonal climatological (1977–2010) sea surface temperature (SST) (Rayner et al., 2003) with generalized surface circulation showing the basin-scale cyclonic gyres during (a) the wet season (SON) and (b) dry (JFM) season. SCS seasonal climatological (1977–2010) sea level pressure (color) with surface level ICOADS (1°) wind direction and relative magnitude (arrows) for (c) the wet season (SON) and (d) dry (JFM) season. The coral site in Hòn Tre, Nha Trang is shown by the star. Surface ocean currents were modified from G. Wang et al. (2006) and K. K. Liu et al. (2002) and include the North Equatorial Current (NEC) and the Indonesian throughflow (ITF). The Luzon Strait is indicated by LS. Winds and sea level pressure data from NOAA (https://psl.noaa.gov/data/gridded/data.coads.1deg.html).

2. Methods

2.1. Study Site

The SCS is one of the largest semi-enclosed marginal seas on the planet (Figure 1). Surface ocean circulation and precipitation are monsoon-driven and change significantly during the year. During the Southwest Monsoon from May to August, relatively stronger winds from the southwest to the northeast establish a strong current moving north-eastward past the sharp continental shelf, leading to regional upwelling along the southern Vietnamese coast (Jilan, 2004) (Note: Southwest Monsoon season not shown in Figure 1). During the Vietnamese wet season (September–November), a double gyre forms, and precipitation is maximal (Figures 1a and 1c). Following the wet season, the Northeast Monsoon or dry season (January–March) winds establish a single gyre pattern of circulation reversing the current along the coast of Vietnam (Figures 1b

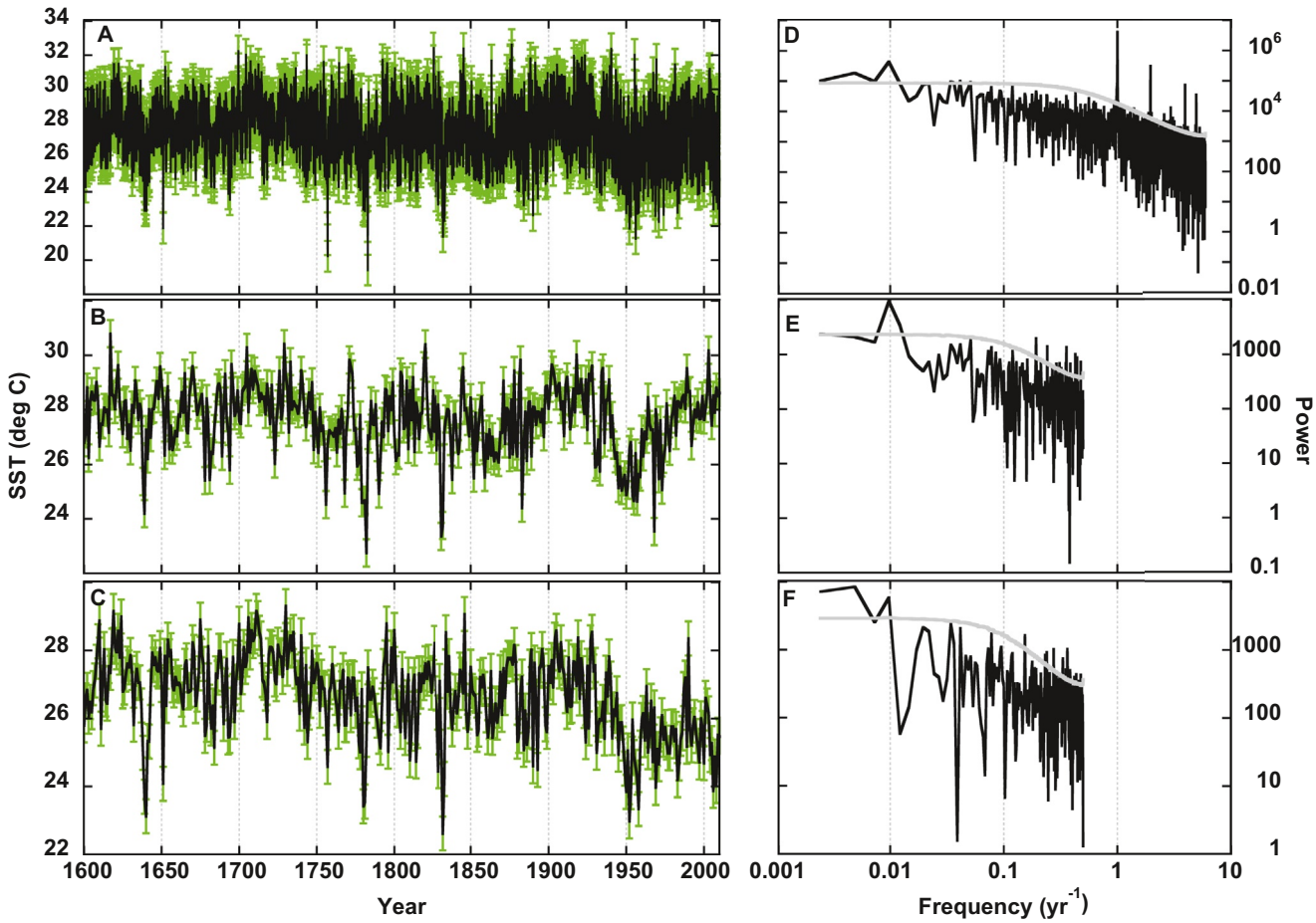

Figure 2. Reconstructed sea surface temperature for (a) monthly, (b) average wet season and (c) average dry season reconstructions. Reconstruction error is shown by green bars. Spectral analysis with 95% confidence (gray) for (d) monthly, (e) wet season, and (f) dry season reconstructions.

and 1d). In addition to circulation changes within the SCS, monsoon winds and regional climate drivers cause changes in the seasonal exchange of water with the Pacific Ocean across the Luzon Strait (C.-T. A. Chen et al., 2015; Jia & Liu, 2004; Nan et al., 2016; Ramos et al., 2019).

To investigate regional changes in SCS hydrography, a massive *Porites* coral was sampled from Hòn Tre Island, off the coast of southern Vietnam (12°12′49.90′′N, 109°18′17.51′′E) in March 2011. An underwater hydraulic drill was used to take a core from the live colony "TN" at 3.6 m water depth, retrieving a continuous record of 4.6 m in length (Bolton et al., 2014). The coral site experiences open ocean conditions and is well-removed from potential runoff from local rivers including the river Cai (Dung et al., 2007; Nguyen et al., 2000) (Figure 1).

2.2. Coral Subsampling and Geochemical Analysis

Coral cores were slabbed into ~1 cm thick pieces and both *x*-rayed and photographed under UV light to reveal density growth bands and luminescent bands affiliated with annual precipitation (Bolton et al., 2014). X-ray images and UV photographs were used both to identify annual bands for age models and to identify optimal growth axes for micro-drilling (Figures S2 and S3). Thin sections were prepared from oriented sections of coral slabs mounted in epoxy resin at both the top and the bottom of coral cores. The thin sections were imaged using a JEOL JSM-7800F Field Emission scanning electron microscopy at Nanyang Technological University (NTU).

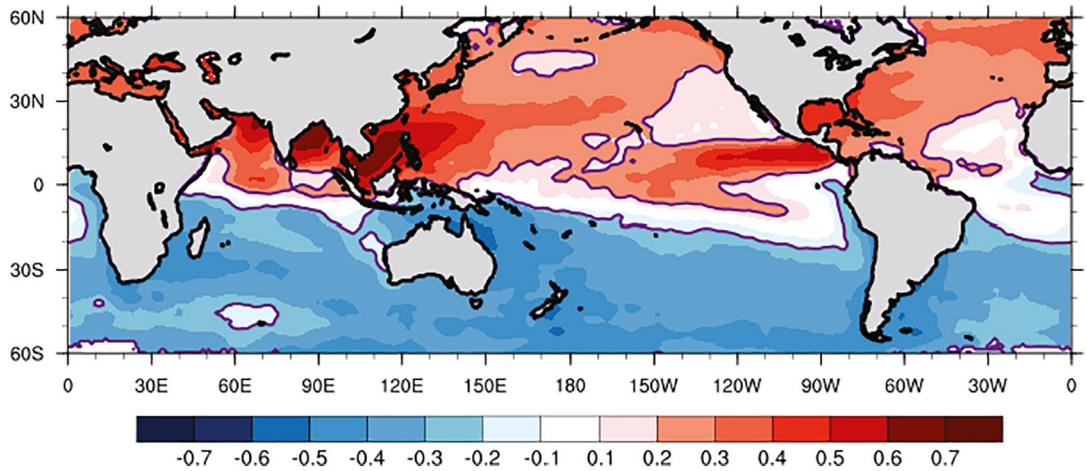

Figure 3. Correlation (r) of coral derived monthly SST to HadISST from 1870 to 2010. Contours indicate regions with 95% confidence level.

Approximately monthly resolution samples were drilled using a 1 mm diameter micro-drill to drill at 0.5 mm intervals to a depth of 1 mm. A sample aliquot of 200–300 μg was then taken for analysis on an Inductively Coupled Plasma Optical Emissions Spectrometer (Thermo iCAP 6000 Series) at NTU. The subsample was dissolved in 2.5 ml of 5% HNO_3 and homogenized for 24 h. Samples were simultaneously measured in triplicate for Sr, Mg, and Ca. Solution standards (0–80 ppm) were routinely measured to correct for instrumental drift and matrix effects from varying calcium concentrations (Schrag, 1999). Two standards were used to evaluate accuracy and precision: a bulk coral powder reference material JCp-1 (Okai et al., 2001) with a consensus Sr/Ca value of 0.01932 (±0.0002) ppm or 8.838 (±0.089) mmol/mol (Hathorne et al., 2013) and an in-house powder standard generated from a fossil coral (*Porites* sp., Bunaken). Repeat measurements of individual aliquots of both powder standards analyzed over a period of 2 years showed very good reproducibility, JCp-1 = 0.019315 (±0.00005) ppm or 8.835 (±0.023) mmol/mol (1σ, relative standard deviation = 0.26%, n = 2125) and Bunaken = 0.019311 (±0.00006) ppm or 8.833 (±0.027) mmol/mol (1σ, relative standard deviation = 0.31%, n = 1202), respectively.

The record from 1977 to 2010 was previously published and calibrated to SST including combined measurements from two adjacent corals (TN–this study and BB–previous study) (Bolton et al., 2014). Beyond the calibration period (1600–1977), the age model was developed by the same methods. Annual dates were assigned using the coral density and luminescent images. Then, the Sr/Ca maxima, minima, and inflection points for each year were paired to the corresponding month from an averaged SST climatology (1977–2010) (Figure S1a) using Analyseries software (Paillard et al., 1996). SST data are from HadISST (HadISST 1.1: Rayner et al., 2003), using the 1° by 1° grid cell centered at 12.5°N, 109.5°E. The Sr/Ca time series was then linearly interpolated to monthly resolution assuming linear growth between tie points. The coral record extends beyond the year 1600; however, noticeably higher average Sr/Ca occurs before 1600, and scanning electron microscopy indicates the presence of secondary aragonite and coral diagenesis (Figure S4). Therefore, we have taken the cautious step of omitting temporal analysis before 1600.

2.3. Conversion to SST

Coral Sr/Ca is converted to SST using the monthly and combined seasonal calibrations of the composite BB and TN previously reported (Bolton et al., 2014). The monthly calibration is:

$$Sr/Ca = -0.055\left(\pm 0.0002\right) * \left(\mathrm{SST}\right) + 10.573\left(\pm 0.430\right) \quad (1)$$

$$r^2 = 0.75,\ p < 0.0001,\ n = 407,\ \mathrm{RMSR} = 0.9°\mathrm{C}$$

and is applied to each linearly interpolated monthly Sr/Ca datum (Figure S1b). RMSR is the root mean square residual of the calibration. The three-month averaged wet (September–November) and dry (Janu-

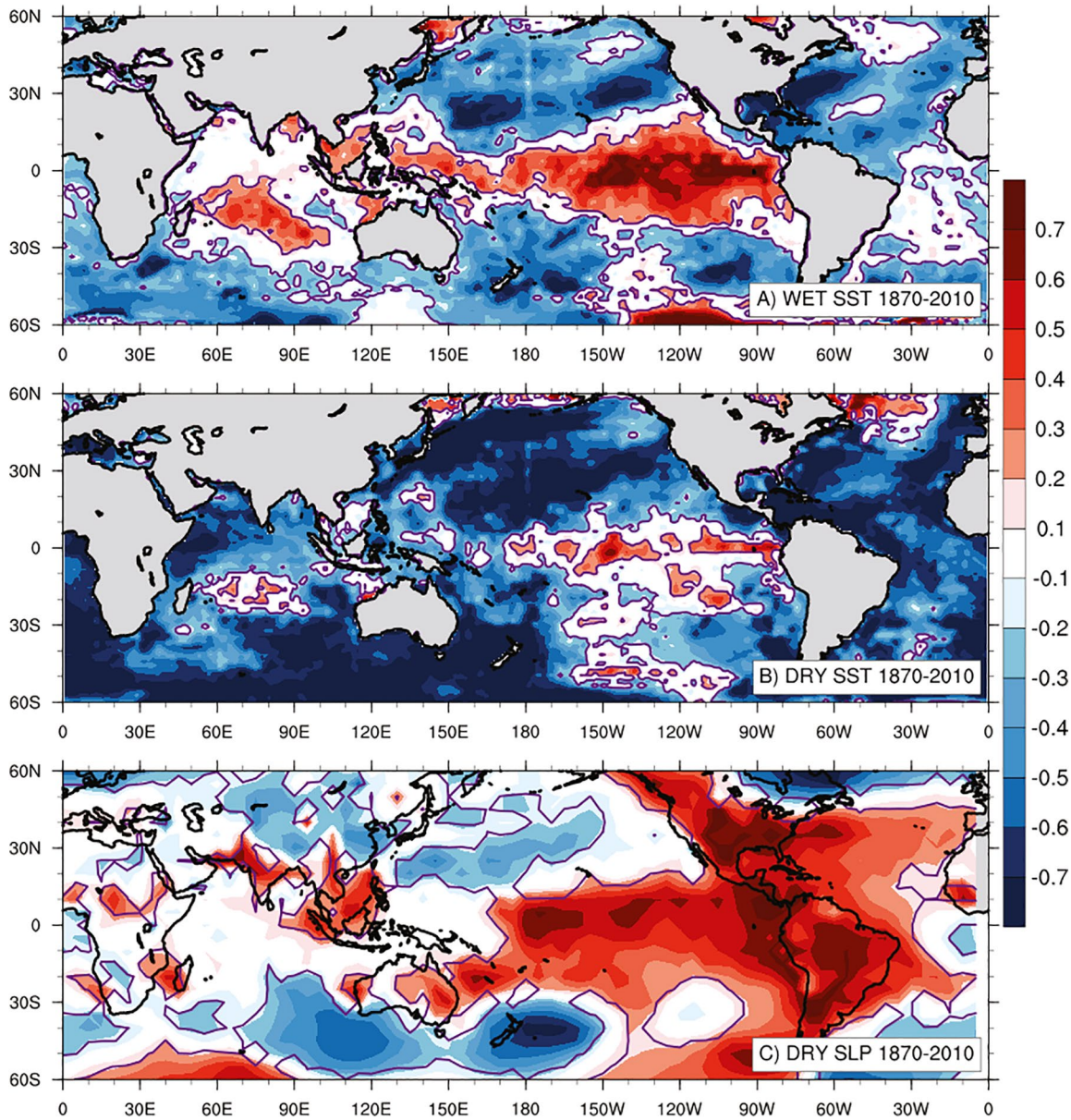

Figure 4. Correlation (r) of coral derived 30-year low-pass filtered (LPF) sea surface temperature (SST) with 30-year LPF global SST and sea level pressure (SLP) during 1870–2010. (a) Coral derived wet season SST correlated to HadISST wet season SST, (b) Coral derived dry season SST correlated to HadISST dry season SST, and (c) Coral derived dry season SST correlated to dry season Hadley SLP. Contours indicate 95% confidence level.

ary–March) seasonal calibration is applied to the corresponding Sr/Ca averages. The seasonal calibration equation is (Figure S1c):

$$Sr/Ca = -0.052\left(\pm 0.0003\right) * \left(\mathrm{SST}\right) + 10.503\left(\pm 0.094\right) \quad (2)$$

$$r^2 = 0.77, p < 0.0001, n = 68, \mathrm{RMSR} = 0.5°\mathrm{C}$$

Note that the dry and wet seasons do not correspond to the SST minima and maxima. The coolest SSTs do occur during the dry season; however, SST maxima occur during boreal summer (June–August, Figure S1)—well before the wet season.

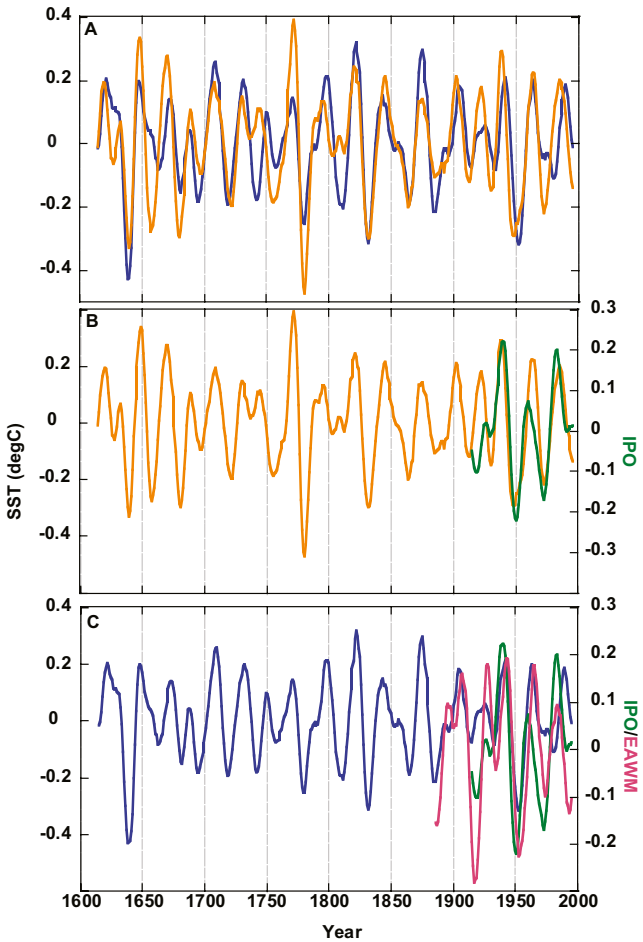

Figure 5. 20–30 year band pass filtered timeseries of coral derived sea surface temperature (SST), instrumental Interdecadal Pacific Oscillation (IPO, Henley et al., 2015), and East Asian Winter Monsoon (EAWM, D'Arrigo, Wilson, Panagiotopoulos, & Wu, 2005). (a) Band pass filtered wet (orange) and dry (blue) season SST, (b) Band pass filtered wet season SST (orange) compared to a similarly filtered IPO index (green), and (c) Band pass filtered dry season SST (blue) compared to similarly filtered IPO index (green) and EAWM index (magenta).

2.4. Statistical Analysis

Power spectra for dry and wet season SST records were calculated using a fast Fourier transform (FFT) with no pre-smoothing and 10,000 Monte Carlo simulations to establish 95% significance using a first-order autoregressive model (i.e., red noise). Wavelet and cross-wavelet analysis were performed using the wavelet coherence methods developed by Grinsted et al. (2004), evaluating 95% confidence against red noise using 300 Monte Carlo simulations. Hamming windows were used to filter each record to 20 and 30 years and the centennial-scale variability is evaluated with a 100-year running mean.

In addition to HadISST, the coral records were compared to ENSO, IPO, and winter EAM (EAWM) indices. The Nino3.4 index from the National Oceanic and Atmospheric Administration (NOAA) (https://psl.noaa.gov/gcos_wgsp/Timeseries/Nino34/) was used to represent ENSO and is based on HadISST. We used the IPO index based on Henley et al., (2015), available from (https://psl.noaa.gov/data/timeseries/IPOTPI/). For the EAWM, we used the D'Arrigo, Wilson, Panagiotopoulos, and Wu (2005) index based on the wind intensity calculated from the Hadley Centre global gridded mean SLP data and using the formula of Wu and Wang (2002). ICOADS surface winds were accessed from https://psl.noaa.gov/data/gridded/data.coads.1deg.html. The NOAA OI v2 satellite SST was accessed from https://psl.noaa.gov/data/gridded/data.noaa.oisst.v2.html.

2.5. Global Climate Models

To evaluate the potential attribution of changed SST patterns to anthropogenic forcing, we utilized the Detection and Attribution Model Intercomparison Project (DAMIP) (Gillett et al., 2016), part of the Coupled Model Intercomparison Project Phase 6 (CMIP6; Eyring et al., 2016). Four simulations of the DAMIP were run, using 30 ensemble members, including configurations with historical, historical natural-only (hist-nat), aerosol-only (AER), and greenhouse gas-only (GHG) boundary conditions. All simulations were evaluated from 1850 to 2014. The historical run includes all forcings, whereas the hist-nat run includes only natural forcings–solar irradiance and stratospheric aerosols. The difference between these two simulations (historical minus hist-nat) isolates the impact of all anthropogenic forcing (anthropogenic; e.g., Ribes et al., 2015). The GHG and AER runs isolate the individual anthropogenic forcings. The comparisons of anthropogenic, GHG, and AER runs allow us to identify specific potential drivers of SST change. Each scenario is presented as the ensemble mean of the 30 common ensemble members of the CanESM5 model (Swart et al., 2019) for the DAMIP/CMIP6 simulations.

To investigate the potential impacts of anthropogenic changes on SST patterns, we employed the High Resolution Model Intercomparison Project (HighResMIP), also part of the CMIP6 (Haarsma et al., 2016), which provides model output at up to 25 km horizontal resolution, critical for investigating marginal seas. The forcing fields of the HighResMIP runs are the same as used in the CMIP6 runs (see Eyring et al. (2016) for details). The HighResMIP monthly historical and future projection data under the socioeconomic pathways 5 (SSP5-85) scenario were used. SSP5-85 is equivalent to representative concentration pathway (RCP) 8.5 and denotes conditions of increased fossil fuel development, thus serving to amplify the anthropogenic forcing. The models were selected based on the availability of ocean heat transport data for both the historical and SSP5 projection periods. We calculated changes by the end of the 21st century (2071–2100 minus 1981–2010) for wet and dry seasons based on a multi-model ensemble, consisting of CNRM-CM6-1-HR (horizontal resolution 25 km; Voldoire et al., 2019), HadGEM3-GC31-MM (horizontal resolution 25 km; Williams et al., 2018), and MPI-ESM1.2-HR (horizontal resolution 40 km; Gutjahr et al., 2019). By showing

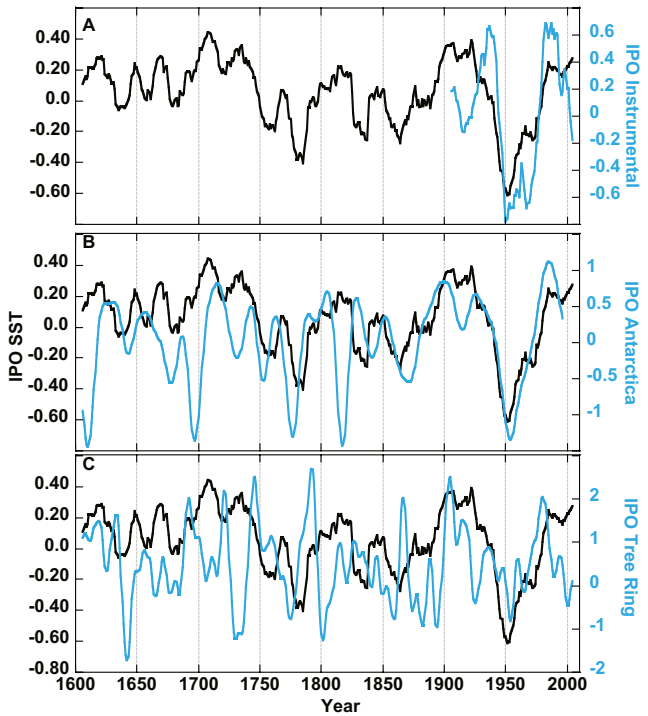

Figure 6. Wet season sea surface temperature coral-generated IPO index (black) compared to (a) the instrumental IPO index (blue, Henley et al., 2015), (b) an Antarctic ice core IPO index (blue, Vance et al., 2015), and (c) a trans-Pacific tree ring-generated IPO index (blue, Buckley et al., 2019).

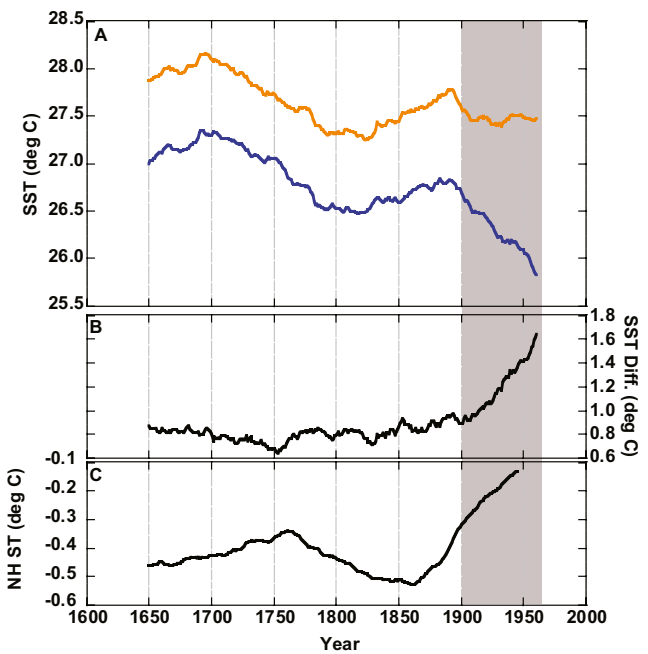

Figure 7. (a) 100-year running average wet (orange) and dry (blue) season sea surface temperature (SST), b) The difference between wet and dry season smoothed SST (gray) and (c) 100-year smoothed northern hemisphere surface air temperature (NH ST, D'Arrigo, Wilson, & Jacoby, 2006). Shaded area denotes the time of decoupling of wet and dry season which coincides with the largest SST seasonal difference and the highest surface temperatures.

the end-of-century changes under the high emission scenario, we highlight the forcing due to anthropogenic climate change.

3. Results

Four hundred years of monthly SSTs from coral Sr/Ca show values from 19.4° to 32.6°C (range of 13.2°C), with the wet season and dry season SST having ranges of 6.6° and 8.0°C respectively between 1600 and 2010 (Figures 2a–2c). Power spectral analysis of each record (monthly, wet, and dry seasons) shows variable power at high frequencies but consistent power across all three time frames at centennial frequencies (Figures 2d–2f). Cross-wavelet analysis between the wet and dry season SSTs shows shared power at greater than 80-year periods and significant correlation at 20–30 and greater than 80-year cycles (Figure S5).

Across the calibration period of 1977–2010, a strong correlation between coral SST and local HadISST is found, as previously reported by Bolton et al. (2014). As we have now greatly extended the record, further comparison to northern hemisphere SST data confirms the strength of our calibration and reliability of the coral records. Monthly SSTs correlate to regional and northern hemisphere SST patterns (Figure 3). When filtered at the 30-year periods identified by the wavelet analysis, wet season SST shows strong correlations to Pacific SSTs that mimics the IPO pattern (Figure 4a), and dry season SST correlates to both IPO SST patterns (Figure 4b) and dry season sea level pressure (SLP) affiliated with the EAWM (Figure 4c).

Twenty-to-thirty-year cycles are identified as a period in which the coral-based SST has elevated shared power and strong spectral coherence between the wet and dry season (Figure S5) and multi-decadal filtered SSTs have strong coherence between proxy and relevant gridded SST fields (Figures 4a and 4b). Therefore, we applied 20–30 year filters to both the wet and dry season SST which shows significant coherence between the two records ($r = 0.71$, $p << 0.0001$), with disagreements in magnitude seen between 1650–1700 and 1750–1800, and in timing around 1750 and the last 50 years (Figure 5a). Significant positive correlations are seen between the wet season record and a similarly filtered IPO record ($r = 0.71$, $p << 0.0001$), and also between dry season SST and both the EAWM (D'Arrigo, Wilson, Panagiotopoulos, & Wu, 2005; Wu & Wang, 2002) and the IPO ($r = 0.58$, $p << 0.0001$ and $r = 0.52$, $p << 0.0001$ respectively) (Figures 5b and 5c). The relationship between dry season SST and the EAWM (Figures 4c and 5c) is inverse of that observed for interannual behavior where a stronger Siberian High results in cooler SSTs in the SCS, but it is consistent with the multi-decadal relationship previously found with ocean circulation proxies (D'Arrigo, Jacoby et al., 2005; Goodkin et al., 2019).

Given the strength of the correlation between the wet season SST and the instrumental IPO, we can isolate a new, long marine IPO index from the wet season SST. Previous paleo-IPO reconstructions focus on 13-year smoothed reconstructions (Cai et al., 2010; Vance et al., 2013), and although this is not a frequency which possesses statistically significant power in our record, we utilize this same smoothing to generate an IPO index comparable to previous reconstructions. The smoothed record is then normalized to 1906–2004, the period for which the instrumental IPO

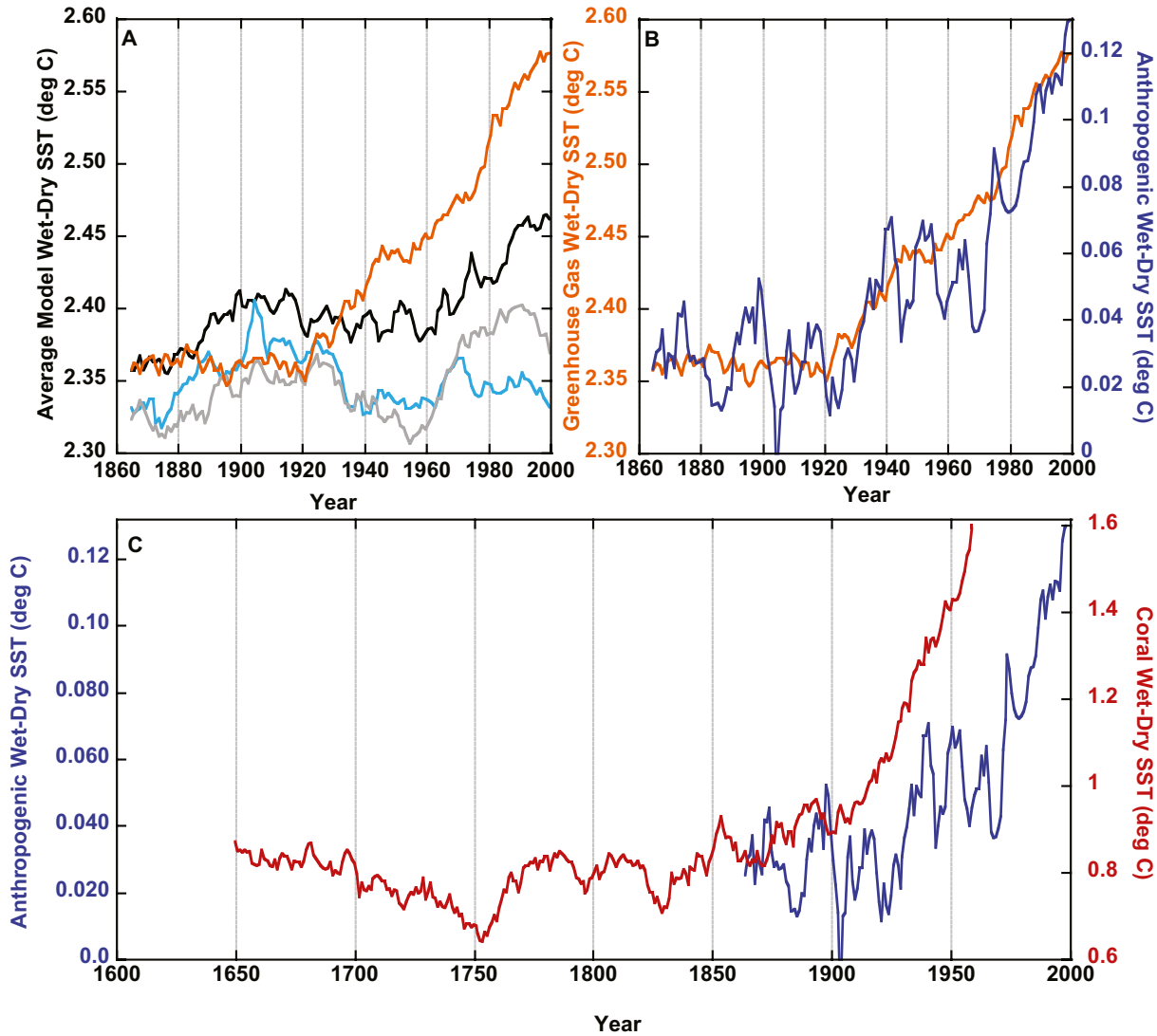

Figure 8. (a) Average wet minus dry sea surface temperature (SST) (°C) versus time for historical (black), hist-nat (light blue), AER (gray), and GHG (orange), (b) Average wet minus dry SST (°C) versus time for GHG (orange) and anthropogenic (blue), and (c) Average wet minus dry SST (°C) versus time for anthropogenic (blue) and the coral (red). The coral records are the 100-year box filter whereas the model data is not long enough for a 100-year filter. Therefore, the model data is shown with a 30-year running mean to preserve the length of the record while smoothing the noise. Anthropogenic = historical minus hist-nat.

is established, by subtracting the mean and dividing by the range. During the period 1906–1996 (the maximum overlap of all records), we show strong, significant correlations with the instrumental IPO ($r = 0.69$, $p << 0.0001$) and an Antarctic based IPO reconstruction (Vance et al., 2015) ($r = 0.86$, $p << 0.0001$), but a weaker correlation to an IPO reconstruction based on tree rings from Vietnam (Buckley et al., 2019) ($r = 0.50$, $p << 0.0001$) (Figures 6a–6c).

Centennial smoothed (100-year running mean) wet and dry season SST records representing the very low-frequency power (Figures 2e and 2f) and the period of strong spectral coherence (Figure S5) show consistent variability over the past 400 years, with very strong correlations across the whole record ($r = 0.86$, $p << 0.0001$), and excluding the record after 1900 ($r = 0.97$, $p << 0.0001$). The increase in correlation when the most recent years are excluded highlights a discrepancy in behavior between the wet and dry seasons visible in the annual and centennial-smoothed records beginning around 1900 (Figures 2b, 2c and 7). While the dry season SST continues to follow a steady cooling trend, the wet season flattens out beginning in 1900 (Figure 7a). Overall,

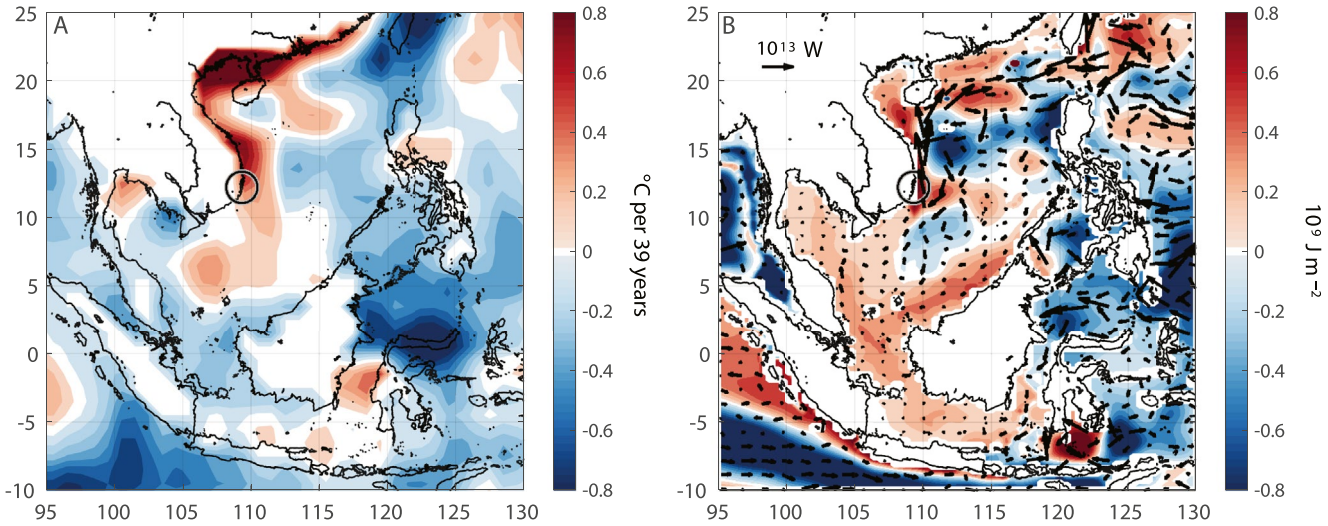

Figure 9. (a) Linear 39-year trend of the difference between wet and dry season sea surface temperature from satellite observation from 1982 to 2020. Large circle centered around coral collection site. (b) The difference in wet and dry season changes (2071–2100 average minus 1981–2010 average) in upper ocean heat content (for top 300 m; in 10^9 J/m^2, color) and the difference in wet and dry season changes (2071–2100 average minus 1981–2010 average) in horizontal heat transport (in 10^{13} W, arrows) both from the multi-model ensemble of HighResMIP models. Future projection is for SSP5-85 scenario.

the difference between wet and dry season SST remains relatively consistent at ~0.8°C until around 1900 when the difference between the two records begins to increase, doubling by the end of the records (Figure 7b), in conjunction with an increase in the northern hemisphere (NH) land temperature (Figure 7c) (D'Arrigo, Wilson, & Jacoby, 2006). After 1900, when the mean NH surface air temperature surpasses its previous maxima, the difference between the wet and dry season SST increases at a rate of 0.76°C per 50 years. Using NOAA OI v2 satellite-based SST (Reynolds et al., 2002), we calculated the difference in SST between the wet and dry season from 1982 to 2020 across the region. The difference along the entire SCS coast is increasing at a rate comparable to what we found in the coral, with the nearest grid box SST difference increasing at a rate of 0.54°C per 39 years (Figure 9a), which extrapolates to a rate of 0.69°C per 50 years.

We hypothesize that the increased difference between wet and dry season SSTs during the twentieth century is due to different responses to anthropogenic warming during the two seasons. To test this, the DAMIP model results were used to isolate the influences of anthropogenic forcing that could lead to a discrepancy in seasonal behavior. Subtracting the hist-nat from the historical simulation results allows an examination of the total anthropogenically driven changes in wet and dry season SST. The total anthropogenic forcing run matches most closely the GHG-only run, indicating that GHGs contribute the most to anthropogenic forcing in the region (Figure 8b). Both the coral and anthropogenic records remain relatively constant until around 1900 when they begin to increase, with the coral record most resembling the consistent SST increase of the GHG only run (Figure 8c). In contrast, the total anthropogenic run increases, plateaus, and then accelerates again, indicating that aerosols have a much smaller role in causing changes to wet-dry season coherence.

These model results do not provide the mechanistic oceanographic changes that lead to this separation in seasonal SST. Therefore, we analyzed the end-of-century changes (2071–2100 minus 1981–2010) across the SCS from the multi-model ensemble of HighResMIP, which essentially reflects the anthropogenically forced changes over the region. End-of-century changes in the models show that heat content increased over the deep basin of the SCS (Figure 9b), with higher accumulation during the wet season than the dry season, particularly around the coral site (Figures 9b and S6a–S6c). While changes to heat transport are larger along the Vietnam coast during the dry season (Figures 9b and S6e), with increased transport through the Luzon Strait and south past our coral site, there is a striking anticyclonic gyre in the wet season around the coral site (relative to dry season; Figures 9b and S6f), indicating greater heat convergence during the wet season. While the HighResMIP ensemble only includes three models, the finding of the anticyclonic gyre is consistent in all three (Figures S7 and S8). These results demonstrate that the impacts of climate change at this location are different between wet and dry seasons and are modulated by changes in heat content and transport, likely driven by changes in regional ocean circulation.

4. Discussion

A distinct change in monthly SST is seen in the variance of the seasonal cycle, with significantly increased variance after 1750 (3.3°C^2) compared to the colder period of the LIA before 1750 (2.0°C^2, $p << 0.0001$) (Figure 2a). Even the variance from 1830 to 1870, the last defined cooling of the LIA (Figure 2b), is 2.4°C^2, significantly smaller than the 1750–2010 variance. While monthly SSTs in the SCS fail to show the severe cooling of the 1600 and 1700s, nor the sharp warming of the 1900s seen in northern latitudes (Bradley & Jones, 1993; D'Arrigo, Wilson, & Jacoby, 2006; Mann et al., 1999), the range of seasonal SSTs at this tropical site experienced significant decreases (increases) during hemispheric cooling (warming).

High-frequency power (<10 years per cycle) appears distributed in all records (Figure 2). Inter-annual variability in this region is very challenging to attribute to climate drivers in large part because the IPO, ENSO, and the EAM are intertwined, with teleconnections that are co-dependent and temporally vary across the SCS (Song & Zhou, 2015). At lower frequencies, the wet and dry season 20–30 year filtered SSTs remain closely coupled throughout the record with some notable exceptions, including a large difference in magnitude of change from 1770 to the early 1800s, and inverted relationships around 1650 and 1750 (Figure 5a). Differences between the dry and wet season SSTs at these frequencies may be the result of modulating influences of the monsoon versus the IPO, as the three periods of disagreement coincide with significantly elevated variance in the winter monsoon (Goodkin et al., 2019). Changes to monsoon winds impact circulation at this site (Figure 1), including winter downwelling, and therefore may impact seasonal SST changes.

Twenty-to-thirty year filtered dry season SST shows a strong positive relationship with both the IPO and the EAWM (Figure 5c). A positive IPO correlating to positive SSTs in the SCS, which is tightly tied to the WPWP, is expected at annual timescales. However, the correlation of the multi-decadal dry season SST to the EAWM (Figures 4c and 5c) is inverse of the anticipated relationship. Modern-day records indicate that as the Siberian High increases and low sea level pressure over the SCS decreases, the EAWM increases and SSTs in the SCS subsequently decrease (inverse to Figures 4c and 5c) (e.g., He et al., 2017). Previous research has also identified an inverse relationship between the EAWM and dry season SCS circulation, suggesting that the multi-decadal variability may have been propagated from the tropical Pacific to the Siberian High (Goodkin et al., 2019). The overall coherence of the IPO to dry season SST and to the EAWM supports the hypothesis that these two systems are tightly coupled at multi-decadal timescales and can lead to unexpected changes in SCS SSTs.

The complexity of the dry season SST relationship to climate drivers is dissimilar from the wet season, which is tightly coupled to the IPO allowing for a new IPO reconstruction (Figure 6). The coral wet season SST-based IPO index and the Antarctic ice core IPO index show very strong agreement (Figure 6b), with most differences occurring when Antarctica shows strong negative IPOs not seen in the SCS (1820, 1690, and 1610s). The Vietnamese tree ring-based IPO record (Figure 6c; Buckley et al., 2019) also does not capture the extreme negative events seen in Antarctica (Figure 6b; Vance et al., 2015), and the tree ring index shows several strong negative IPOs not recorded in either the coral or Antarctic records (1880–1890, 1800, 1730, and 1640s). The recording of negative IPOs by some proxies and not by others is an indication that perhaps the negative phase of the IPO is less geographically stationary through time. Over the length of the instrumental record, Antarctica is more sensitive to the negative IPO state, showing the lowest values, and the tree rings show higher frequency behavior than the other two reconstructions (Figure 6; Buckley et al., 2019; Vance et al., 2015). The coral IPO record shows a significant decrease in variance during the heart of the LIA (1606–1750) compared to post-1750 (0.02°C^2, 0.05°C^2, $p << 0.001$), with no significant negative phase during the LIA. While the other two IPO reconstructions have less agreement during this period, they do not show a significant decline in variance. As the coral site is very sensitive to the EAM, and the LIA is known to lead to a more variable monsoon (Goodkin et al., 2019), this may have led to a dampening of the IPO impact on the coral site during this period.

Centennial scale variability, which shows very strong power in all three records (monthly, wet and dry season, Figure 2), dominates SST behavior at this location and is likely the reason why widespread northern hemispheric surface temperature patterns are not observed. For 300 years, the wet and dry seasons are tightly coupled, with a pattern of rising temperatures followed by a slow decline and another increase

(Figure 7a). Around 1900, the dry season SST continues the anticipated decline whereas the wet season SST becomes relatively constant (Figure 7a). The decoupling of the records is highlighted by the sharp increase in the seasonal SST difference (Figure 7b). Prior to about 1900, the difference between the records was relatively constant with an average of ~0.8°C, but increased by a factor of two by the end of the record. The SST offset increased together with the rapid increase in northern hemispheric temperatures widely attributed to greenhouse gas forcing (Figure 7c) (Mann et al., 1999), and in agreement with DAMIP ensemble simulations identifying the greatest twentieth century increase in wet–dry SST difference resulting from the GHG-only run (Figure 8a).

The decoupling of centennial-scale SST variability between the wet and dry seasons appears to be driven by a change in climate behavior and ocean circulation differently impacting the wet season through time. This is illustrated by an increasing divergence between seasonal SSTs in both the coral record and satellite SST data across the entire northern coast of the SCS (Figure 9a). Examining the HighResMIP models shows that by the end of the 21st century the heat content in the upper ocean in the western SCS is expected to increase during both the wet and dry seasons. However, larger increases are likely to occur during the wet season (~0.8 G J/m^2 around the coral site) (Figures S6a and S6b). Simultaneously, horizontal heat transport is expected to increase in both seasons from ~2000 to ~2100, with an increase in transport across the Luzon Strait from the western Pacific (Figures S6d and S6e) as also seen in a regional study (Samanta et al., 2021). In the dry season, this transport continues to the southwest across the SCS and past the coral site, likely under the influence of the winter monsoon winds (Figure 1d). In the wet season, however, when the winds are less well-formed (Figure 1c) (Jilan, 2004), the heat transport dissipates within the SCS with an anticyclonic gyre forming along the western coast, likely leading to relatively increased heat content in the wet season in this region (Figures 9b and S6).

The presence of centennial-scale SST variability in the western SCS during both wet and dry seasons is an indication that such low-frequency climate forcing is an important component of natural climate variability in this key region for global climate (Karnauskas et al., 2012). The recent decoupling of the wet and dry season SST after 300 years of synchronized behavior is an ominous warning that even patterns of climate variability that were stable over long periods can shift abruptly, with long-lasting consequences for regional hydroclimate and ultimately society. Although reconstructed wet-dry season SST differences have more than doubled since ~1900, climate model attribution indicates that GHG is the major driver of these changes and climate model simulations of high-emission scenarios show that these impacts may be amplified in the future. Additional multi-century records from corals sensitive to important climate systems are critical to identifying multidecadal-to-centennial scale patterns of internal variability and evaluating potential changes due to anthropogenic forcing.

Data Availability Statement

Coral data will be archived at the NOAA Paleoclimate Data Center (https://www.ncdc.noaa.gov/paleo/study/32392) and are available in excel as Data Set S1. NOAA OI SST v2 data are available from https://psl.noaa.gov/data/gridded/data.noaa.oisst.v2.highres.html. HadISST data are available from https://www.metoffice.gov.uk/hadobs/hadisst/. CMIP6 HighResMIP and DAMIP model data are available from https://esgf-node.llnl.gov/search/cmip6.

References

Abram, N. J., McGregor, H. V., Gagan, M. K., Hantoro, W. S., & Suwargadi, B. W. (2009). Oscillations in the southern extent of the Indo-Pacific Warm Pool during the mid-Holocene. *Quaternary Science Reviews*, *28*(25–26), 2794–2803. https://doi.org/10.1016/j.quascirev.2009.07.006

Alibert, C., & McCulloch, M. T. (1997). Strontium/calcium ratios in modern Porites corals from the Great Barrier Reef as a proxy for sea surface temperature: Calibration of the thermometer and monitoring of ENSO. *Paleoceanography*, *12*(3), 345–363. https://doi.org/10.1029/97pa00318

Beck, J. W., Edwards, R. L., Ito, E., Taylor, F. W., Recy, J., Rougerie, F., et al. (1992). Sea-surface temperature from coral skeletal strontium calcium ratios. *Science*, *257*(5070), 644–647. https://doi.org/10.1126/science.257.5070.644

Bolton, A., Goodkin, N. F., Hughen, K., Ostermann, D. R., Vo, S. T., & Phan, H. K. (2014). Paired Porites coral Sr/Ca and delta O-18 from the western South China Sea: Proxy calibration of sea surface temperature and precipitation. *Palaeogeography, Palaeoclimatology, Palaeoecology*, *410*, 233–243. https://doi.org/10.1016/j.palaeo.2014.05.047

Acknowledgments
Thanks to G. Williams, W. Tak-Cheung, and J. Ossolinski for assistance with field work which was funded in part by a WHOI Access to the Sea Grant. The authors acknowledge the World Climate Research Programme, which, through its Working Group on Coupled Modelling, coordinated and promoted CMIP6. The authors thank the climate modelling groups for producing and making available their model output, the Earth System Grid Federation (ESGF) for archiving the data and providing access, and the multiple funding agencies that support CMIP6 and ESGF. This research was supported by a Singapore National Research Fellowship to N.F. Goodkin (NRFF-2012-03) as administered by the Earth Observatory of Singapore and by a Singapore Ministry of Education Academic Research Fund Tier 2 award to N.F. Goodkin, K.A. Hughen, and K.B. Karnauskas (MOE-2016-T2-1-016). D. Samanta was partially supported by a Singapore Ministry of Education Tier 3 award (MOE2019-T3-1-004). This manuscript was improved with the comments of two anonymous reviewers. This is EOS contribution number 386.

Bradley, R. S., & Jones, P. D. (1993). Little Ice Age summer temperature variations: Their nature and relevance to recent global warming trends. *The Holocene*, *3*(4), 367–376. https://doi.org/10.1177/095968369300300409
Buckley, B. M., Fletcher, R., Wang, S. Y. S., Zottoli, B., & Pottier, C. (2014). Monsoon extremes and society over the past millennium on mainland Southeast Asia. *Quaternary Science Reviews*, *95*, 1–19. https://doi.org/10.1016/j.quascirev.2014.04.022
Buckley, B. M., Ummenhofer, C. C., D'Arrigo, R. D., Hansen, K. G., Truong, L. H., Le, C. N., & Stahle, D. K. (2019). Interdecadal Pacific Oscillation reconstructed from trans-Pacific tree rings: 1350–2004 CE. *Climate Dynamics*, *53*(5–6), 3181–3196. https://doi.org/10.1007/s00382-019-04694-4
Cai, W., van Rensch, P., Cowan, T., & Sullivan, A. (2010). Asymmetry in ENSO teleconnection with regional rainfall, its multidecadal variability, and impact. *Journal of Climate*, *23*(18), 4944–4955. https://doi.org/10.1175/2010jcli3501.1
Carilli, J. E., McGregor, H. V., Gaudry, J. J., Donner, S. D., Gagan, M. K., Stevenson, S., et al. (2014). Equatorial Pacific coral geochemical records show recent weakening of the Walker Circulation. *Paleoceanography*, *29*(11), 1031–1045. https://doi.org/10.1002/2014pa002683
Chen, C.-T. A., Yeh, Y.-T., Chen, Y.-C., & Huang, T.-H. (2015). Seasonal and ENSO-related interannual variability of subsurface fronts separating West Philippine Sea waters from South China Sea waters near the Luzon Strait. *Deep-Sea Research Part I: Oceanographic Research Papers*, *103*, 13–23. https://doi.org/10.1016/j.dsr.2015.05.002
Chen, D., Zhou, F. F., Dong, Z. P., Zeng, A., Ou, T. H., & Fang, K. Y. (2020). A tree-ring delta O-18 based reconstruction of East Asia summer monsoon over the past two centuries. *PloS One*, *15*(6), 15. https://doi.org/10.1371/journal.pone.0234421
Cole, J. E., Fairbanks, R. G., & Shen, G. T. (1993). Recent variability in the Southern Oscillation—Isotopic results from a Tarawa Atoll coral. *Science*, *260*(5115), 1790–1793. https://doi.org/10.1126/science.260.5115.1790
Cravatte, S., Delcroix, T., Zhang, D., McPhaden, M., & Leloup, J. (2009). Observed freshening and warming of the western Pacific Warm Pool. *Climate Dynamics*, *33*(4), 565–589. https://doi.org/10.1007/s00382-009-0526-7
Crueger, T., Zinke, J., & Pfeiffer, M. (2009). Patterns of Pacific decadal variability recorded by Indian Ocean corals. *International Journal of Earth Sciences*, *98*(1), 41–52. https://doi.org/10.1007/s00531-008-0324-1
D'Arrigo, R., Jacoby, G., Wilson, R., & Panagiotopoulos, F. (2005). A reconstructed Siberian High index since A. D. 1599 from Eurasian and North American tree rings. *Geophysical Research Letters*, *32*(5), 4. https://doi.org/10.1029/2004gl022271
D'Arrigo, R., & Ummenhofer, C. C. (2015). The climate of Myanmar: Evidence for effects of the Pacific Decadal Oscillation. *International Journal of Climatology*, *35*(4), 634–640. https://doi.org/10.1002/joc.3995
D'Arrigo, R., Wilson, R., Deser, C., Wiles, G., Cook, E., Villalba, R., et al. (2005). Tropical-North Pacific climate linkages over the past four centuries. *Journal of Climate*, *18*(24), 5253–5265. https://doi.org/10.1175/JCLI3602.1
D'Arrigo, R., Wilson, R., & Jacoby, G. (2006). On the long-term context for late twentieth century warming. *Journal of Geophysical Research*, *111*(D3). https://doi.org/10.1029/2005jd006352
D'Arrigo, R., Wilson, R., Palmer, J., Krusic, P., Curtis, A., Sakulich, J., et al. (2006). The reconstructed Indonesian warm pool sea surface temperatures from tree rings and corals: Linkages to Asian monsoon drought and El Niño-Southern Oscillation. *Paleoceanography*, *21*(3), PA3005. https://doi.org/10.1029/2005PA001256
D'Arrigo, R., Wilson, R., Panagiotopoulos, F., & Wu, B. Y. (2005). On the long-term interannual variability of the East Asian winter monsoon. *Geophysical Research Letters*, *32*(21). https://doi.org/10.1029/2005gl023235
DeLong, K. L., Flannery, J. A., Poore, R. Z., Quinn, T. M., Maupin, C. R., Lin, K., & Shen, C.-C. (2014). A reconstruction of sea surface temperature variability in the Southeastern Gulf of Mexico from 1734 to 2008 CE. using cross-dated Sr/Ca records from the coral Siderastrea siderea. *Paleoceanography*, *29*(5), 403–422. https://doi.org/10.1002/2013pa002524
DeLong, K. L., Quinn, T. M., Taylor, F. W., Lin, K., & Shen, C.-C. (2012). Sea surface temperature variability in the southwest tropical Pacific since AD 1649. *Nature Climate Change*, *2*(11), 799–804. https://doi.org/10.1038/nclimate1583
DeLong, K. L., Quinn, T. M., Taylor, F. W., Shen, C. C., & Lin, K. (2013). Improving coral-base paleoclimate reconstructions by replicating 350years of coral Sr/Ca variations. *Palaeogeography, Palaeoclimatology, Palaeoecology*, *373*, 6–24. https://doi.org/10.1016/j.palaeo.2012.08.019
Deng, W., Liu, X., Chen, X., Wei, G., Zeng, T., Xie, L., & Zhao, J.-x. (2017). A comparison of the climates of the Medieval Climate Anomaly, Little Ice Age, and Current Warm Period reconstructed using coral records from the northern South China Sea. *Journal of Geophysical Research: Oceans*, *122*(1), 264–275. https://doi.org/10.1002/2016jc012458
Deng, W., Wei, G., Xie, L., Ke, T., Wang, Z., Zeng, T., & Liu, Y. (2013). Variations in the Pacific Decadal Oscillation since 1853 in a coral record from the northern South China Sea. *Journal of Geophysical Research: Oceans*, *118*(5), 2358–2366. https://doi.org/10.1002/jgrc.20180
de Villiers, S., Shen, G. T., & Nelson, B. K. (1994). The Sr/Ca-temperature relationship in coralline Aragonite—Influence of variability in (Sr/Ca) seawater and skeletal growth-parameters. *Geochimica et Cosmochimica Acta*, *58*(1), 197–208. https://doi.org/10.1016/0016-7037(94)90457-x
Dunbar, R. B., & Cole, J. E. (1999). *Annual records of tropical systems (ARTS)*. (PAGES Workshop Report).
Dung, L. D. (2007). *The marine protected area of Nha Trang Bay, Vietnam: Initial trends in the resource status and utlization (2002–2005)*. Norway: University of Tromso.
Eyring, V., Gleckler, P. J., Heinze, C., Stouffer, R. J., Taylor, K. E., Balaji, V., et al. (2016). Towards improved and more routine Earth system model evaluation in CMIP. *Earth System Dynamics*, *7*(4), 813–830. https://doi.org/10.5194/esd-7-813-2016
Gagan, M. K., Ayliffe, L. K., Opdyke, B. N., Hopley, D., Scott-Gagan, H., & Cowley, J. (2002). Coral oxygen isotope evidence for recent groundwater fluxes to the Australian Great Barrier Reef. *Geophysical Research Letters*, *29*(20). https://doi.org/10.1029/2002gl015336
Gillett, N. P., Shiogama, H., Funke, B., Hegerl, G., Knutti, R., Matthes, K., et al. (2016). The detection and attribution model intercomparison project (DAMIP v1.0) contribution to CMIP6. *Geoscientific Model Development*, *9*(10), 3685–3697. https://doi.org/10.5194/gmd-9-3685-2016
Goodkin, N. F., Bolton, A., Hughen, K. A., Karnauskas, K. B., Griffin, S., Phan, K. H., et al. (2019). East Asian monsoon variability since the sixteenth century. *Geophysical Research Letters*, *46*(9), 4790–4798. https://doi.org/10.1029/2019gl081939
Goodkin, N. F., Hughen, K. A., Curry, W. B., Doney, S. C., & Ostermann, D. R. (2008). Sea surface temperature and salinity variability at Bermuda during the end of the Little Ice Age. *Paleoceanography*, *23*(3). https://doi.org/10.1029/2007pa001532
Goodkin, N. F., Wang, B. S., You, C. F., Hughen, K. A., Grumet-Prouty, N., Bates, N. R., & Doney, S. C. (2015). Ocean circulation and biogeochemistry moderate interannual and decadal surface water pH changes in the Sargasso Sea. *Geophysical Research Letters*, *42*(12), 4931–4939. https://doi.org/10.1002/2015gl064431
Griffiths, M. L., Kimbrough, A. K., Gagan, M. K., Drysdale, R. N., Cole, J. E., Johnson, K. R., et al. (2016). Western Pacific hydroclimate linked to global climate variability over the past two millennia. *Nature Communications*, *7*. https://doi.org/10.1038/ncomms11719
Grinsted, A., Moor, J. C., & Jevrejeva, S. (2004). Application of the cross wavelet transform and wavelet coherence to geophysical time series. *Nonlinear Processes in Geophysics*, *11*(5/6), 561–566. https://doi.org/10.5194/npg-11-561-2004

Gutjahr, O., Putrasahan, D., Lohmann, K., Jungclaus, J. H., Von Storch, J. S., Brüggemann, N., et al. (2019). Max Planck Institute Earth System Model (MPI-ESM1.2) for the High-Resolution Model Intercomparison Project (HighResMIP). *Geoscientific Model Development*, *12*(7), 3241–3281. https://doi.org/10.5194/gmd-12-3241-2019

Haarsma, R. J., Roberts, M. J., Vidale, P. L., Senior, C. A., Bellucci, A., Bao, Q., et al. (2016). High Resolution Model Intercomparison Project (HighResMIP v1.0) for CMIP6. *Geoscientific Model Development*, *9*(11), 4185–4208. https://doi.org/10.5194/gmd-9-4185-2016

Hathorne, E. C., Gagnon, A., Felis, T., Adkins, J., Asami, R., Boer, W., et al. (2013). Interlaboratory study for coral Sr/Ca and other element/Ca ratio measurements. *Geochemistry, Geophysics, Geosystems*, *14*, 3730–3750. https://doi.org/10.1002/ggge.20230

He, S., Gao, Y., Li, F., Wang, H., & He, Y. (2017). Impact of Arctic Oscillation on the East Asian climate: A review. *Earth-Science Reviews*, *164*, 48–62. https://doi.org/10.1016/j.earscirev.2016.10.014

Henley, B. J., Gergis, J., Karoly, D. J., Power, S., Kennedy, J., Folland, C. K. (2015). A Tripole Index for the Interdecadal Pacific Oscillation, *Climate Dynamics 45*:3077–3090. https://doi.org/10.1007/s00382-015-2525-1

Hu, Z. Z., Bengtsson, L., & Arpe, K. (2000). Impact of global warming on the Asian winter monsoon in a coupled GCM. *Journal of Geophysical Research*, *105*(D4), 4607–4624. https://doi.org/10.1029/1999jd901031

Hughen, K. A., Schrag, D. P., Jacobsen, S. B., & Hantoro, W. (1999). El Niño during the last interglacial period recorded by a fossil coral from Indonesia. *Geophysical Research Letters*, *26*(20), 3129–3132. https://doi.org/10.1029/1999gl006062

Jia, Y. L., & Liu, Q. Y. (2004). Eddy shedding from the Kuroshio bend at Luzon Strait. *Journal of Oceanography*, *60*(6), 1063–1069. https://doi.org/10.1007/s10872-005-0014-6

Jilan, S. (2004). Overview of the South China Sea circulation and its influence on the coastal physical oceanography outside the Pearl River Estuary. *Continental Shelf Research*, *24*(16), 1745–1760. https://doi.org/10.1016/j.csr.2004.06.005

Karnauskas, K. B., Smerdon, J. E., Seager, R., & Gonzalez-Rouco, J. F. (2012). A Pacific Centennial Oscillation predicted by coupled GCMs. *Journal of Climate*, *25*(17), 5943–5961. https://doi.org/10.1175/jcli-d-11-00421.1

Kilbourne, K. H., Quinn, T. M., Webb, R., Guilderson, T., Nyberg, J., & Winter, A. (2010). Coral windows onto seasonal climate variability in the northern Caribbean since 1479. *Geochemistry, Geophysics, Geosystems*, *11*(10), Q10006. https://doi.org/10.1029/2010gc003171

Klein, S. A., Soden, B. J., & Lau, N. C. (1999). Remote sea surface temperature variations during ENSO: Evidence for a tropical atmospheric bridge. *Journal of Climate*, *12*(4), 917–932. https://doi.org/10.1175/1520-0442(1999)012<0917:rsstvd>2.0.co;2

Lau, K. M., & Li, M. T. (1984). The monsoon of East-Asia and its global associations—A survey. *Bulletin of the American Meteorological Society*, *65*(2), 114–125. https://doi.org/10.1175/1520-0477(1984)065<0114:tmoeaa>2.0.co;2

Lau, N. C. (1997). Interactions between global SST anomalies and the midlatitude atmospheric circulation. *Bulletin of the American Meteorological Society*, *78*(1), 21–33. https://doi.org/10.1175/1520-0477(1997)078<0021:ibgsaa>2.0.co;2

Li, H., Dai, A., Zhou, T., & Lu, J. (2010). Responses of the East Asian summer monsoon to historical SST and atmospheric forcing during 1950–2000. *Climate Dynamics*, *34*, 501–514. https://doi.org/10.1007/s00382-008-0482-7

Li, Y. Q., & Yang, S. (2010). A dynamical index for the East Asian winter monsoon. *Journal of Climate*, *23*(15), 4255–4262. https://doi.org/10.1175/2010jcli3375.1

Liu, C. C., Yan, H., Fei, H. B., Ma, X. L., Zhang, W. C., Shi, G., et al. (2019). Temperature seasonality and ENSO variability in the northern South China Sea during the Medieval Climate Anomaly interval derived from the Sr/Ca ratios of Tridacna shell. *Journal of Asian Earth Sciences*, *180*, 9. https://doi.org/10.1016/j.jseaes.2019.103880

Liu, J., Chen, J., Zhang, X., Li, Y., Rao, Z., & Chen, F. (2015). Holocene East Asian summer monsoon records in northern China and their inconsistency with Chinese stalagmite δ18O records. *Earth-Science Reviews*, *148*, 194–208. https://doi.org/10.1016/j.earscirev.2015.06.004

Liu, K. K., Chao, S. Y., Shaw, P. T., Gong, G. C., Chen, C. C., & Tang, T. Y. (2002). Monsoon-forced chlorophyll distribution and primary production in the South China Sea: Observations and a numerical study. *Deep Sea Research Part I: Oceanographic Research Papers*, *49*(8), 1387-1412. https://doi.org/10.1016/S0967-0637(02)00035-3

Mann, M. E., Bradley, R. S., & Hughes, M. K. (1999). Northern hemisphere temperatures during the past millennium: Inferences, uncertainties, and limitations. *Geophysical Research Letters*, *26*(6), 759–762. https://doi.org/10.1029/1999gl900070

Mitsuguchi, T., Dang, P. X., Kitagawa, H., Uchida, T., & Shibata, Y. (2008). Coral Sr/Ca and Mg/Ca records in Con Dao Island off the Mekong Delta: Assessment of their potential for monitoring ENSO and East Asian monsoon. *Global and Planetary Change*, *63*(4), 341–352. https://doi.org/10.1016/j.gloplacha.2008.08.002

Moberg, A., Sonechkin, D. M., Holmgren, K., Datsenko, N. M., Karlen, W., & Lauritzen, S. E. (2006). Highly variable Northern Hemisphere temperatures reconstructed from low- and high-resolution proxy data. *Nature*, *439*(7079), 1014–1014. https://doi.org/10.1038/nature04575

Morton, B., & Blackmore, G. (2001). South China Sea. *Marine Pollution Bulletin*, *42*(12), 1236–1263. https://doi.org/10.1016/s0025-326x(01)00240-5

Nan, F., Yu, F., Xue, H., Zeng, L., Wang, D., Yang, S., & Kim-Cuong, N. (2016). Freshening of the upper ocean in the South China Sea since the early 1990s. *Deep-Sea Research Part I: Oceanographic Research Papers*, *118*, 20–29. https://doi.org/10.1016/j.dsr.2016.10.010

Newton, A., Thunell, R., & Stott, L. (2006). Climate and hydrographic variability in the Indo-Pacific Warm Pool during the last Millenium. *Geophysical Research Letters*, *33*. https://doi.org/10.1029/2006gl027234

Nguyen, T. A., Vo, D. S., Phan, M. T., Nguyen, H. H., & Ittekott, V. (2000). Tracing sediment transport and bed regime in Nha Trang Bay. *Collection of Marine Research Works*, *10*, 63–69.

Okai, T., Suzuki, A., Kawahata, H., Terashima, S., Imai, N. (2001). Preparation of a new geological survey of Japan geochemical reference material: Coral JCp-1. *Geostandards Newsletter*, *26*, 95–99.

Paillard, D., Labeyrie, L., & Yiou, P. (1996). Macintosh program performs time-series analysis. *Eos, Transactions American Geophysical Union*, *77*(39), 379–379. https://doi.org/10.1029/96eo00259

Power, S., Casey, T., Folland, C., Colman, A., & Mehta, V. (1999). Inter-decadal modulation of the impact of ENSO on Australia. *Climate Dynamics*, *15*(5), 319–324. https://doi.org/10.1007/s003820050284

Ramos, R. D., Goodkin, N. F., Druffel, E. R. M., Fan, T. Y., & Siringan, F. P. (2019). Interannual coral delta C-14 records of surface water exchange across the Luzon Strait. *Journal of Geophysical Research: Oceans*, *124*(1), 491–505. https://doi.org/10.1029/2018jc014735

Ramos, R. D., Goodkin, N. F., & Fan, T. Y. (2020). Coral records at the northern edge of the Western Pacific Warm Pool reveal multiple drivers of sea surface temperature, salinity, and rainfall variability since the end of the Little Ice Age. *Paleoceanography and Paleoclimatology*, *35*(5), 21. https://doi.org/10.1029/2019pa003826

Rayner, N. A., Parker, D. E., Horton, E. B., Folland, C. K., Alexander, L. V., Rowell, D. P., et al. (2003). Global analyses of sea surface temperature, sea ice, and night marine air temperature since the late nineteenth century. *Journal of Geophysical Research*, *108*(D14). https://doi.org/10.1029/2002JD002670

Ren, H. J., Chen, Y. C., Wang, X. T., Wong, G. T. F., Cohen, A. L., DeCarlo, T. M., et al. (2017). 21st-century rise in anthropogenic nitrogen deposition on a remote coral reef. *Science*, *356*(6339), 749–752. https://doi.org/10.1126/science.aal3869
Reynolds, R. W., Rayner, N. A., Smith, T. M., Stokes, D. C., & Wang, W. Q. (2002). An improved in situ and satellite SST analysis for climate. *Journal of Climate*, *15*(13), 1609–1625. https://doi.org/10.1175/1520-0442(2002)015<1609:aiisas>2.0.co;2
Ribes, A., Gillett, N. P., & Zwiers, F. W. (2015). Designing detection and attribution simulations for CMIP6 to optimize the estimation of greenhouse gas–induced warming. *Journal of Climate*, *28*(8), 3435–3438. https://doi.org/10.1175/jcli-d-14-00691.1
Salinger, M. J., Renwick, J. A., & Mullan, A. B. (2001). Interdecadal Pacific Oscillation and South Pacific climate. *International Journal of Climatology*, *21*(14), 1705–1721. https://doi.org/10.1002/joc.691
Samanta, D., Goodkin, N. F., & Karnauskas, K. B. (2021). Volume and heat transport in the South China Sea and maritime continent at present and the end of the 21st century. *Journal of Geophysical Research: Oceans*, *126*, e2020JC016901. https://doi.org/10.1029/2020JC016901
Samanta, D., Karnauskas, K. B., Goodkin, N. F., Coats, S., Smerdon, J. E., & Zhang, L. (2018). Coupled model biases breed spurious low-frequency variability in the tropical Pacific Ocean. *Geophysical Research Letters*, *45*(19), 10609–10618. https://doi.org/10.1029/2018gl079455
Samanta, D., Rajagopalan, B., Karnauskas, K. B., Zhang, L., & Goodkin, N. F. (2020). La Nina's diminishing fingerprint on the central Indian Summer Monsoon. *Geophysical Research Letters*, *47*(2), 11. https://doi.org/10.1029/2019gl086237
Schrag, D. P. (1999). Rapid analysis of high-precision Sr/Ca ratios in corals and other marine carbonates. *Paleoceanography*, *14*(2), 97–102.
Smith, S. V., Buddemeier, R. W., Redalje, R. C., & Houck, J. E. (1979). Strontium-Calcium Thermometry in Coral Skeletons. *Science*, *204*(4391), 404–407. https://doi.org/10.1126/science.204.4391.404
Song, F., & Zhou, T. (2014). Internanual variability or East Asian Summer Monsoon simulated by CMIP3 and CMIP5 AGCMs: Skill dependence on Indian Ocean-Western Pacific anticyclone teleconnection. *Journal of Climate*, *27*, 1679–1697. https://doi.org/10.1175/jcli-d-13-00248.1
Song, F., & Zhou, T. (2015). The dominant role of internal variability in modulating the decadal variation of the East Asian summer monsoon-ENSO relationship during the 20th century. *Journal of Climate*, *28*, 7093–7107. https://doi.org/10.1175/jcli-d-14-00783.1
Song, S. H., Peng, Z. C., Zhou, W. J., Liu, W. G., Liu, Y., & Chen, T. G. (2012). Variation of the winter monsoon in South China Sea over the past 183 years: Evidence from oxygen isotopes in coral. *Global and Planetary Change*, *98–99*, 131–138. https://doi.org/10.1016/j.gloplacha.2012.08.013
Swart, N. C., Cole, J. N., Kharin, V. V., Lazare, M., Scinocca, J. F., Gillett, N. P., et al. (2019). The Canadian earth system model version 5 (CanESM5. 0.3). *Geoscientific Model Development*, *12*(11), 4823–4873. https://doi.org/10.5194/gmd-12-4823-2019
United Nations. (2019). *World population prospects*. Retrieved From Department of Economic and Social Affairs Population Division https://population.un.org/wpp/Download/Standard/Population/
Vance, T. R., Roberts, J. L., Plummer, C. T., Kiem, A. S., & van Ommen, T. D. (2015). Interdecadal Pacific variability and eastern Australian megadroughts over the last millennium. *Geophysical Research Letters*, *42*(1), 129–137. https://doi.org/10.1002/2014gl062447
Vance, T. R., van Ommen, T. D., Curran, M. A. J., Plummer, C. T., & Moy, A. D. (2013). A Millennial proxy record of ENSO and Eastern Australian rainfall from the Law Dome Ice Core, East Antarctica. *Journal of Climate*, *26*(3), 710–725. https://doi.org/10.1175/jcli-d-12-00003.1
Voldoire, A., Saint-Martin, D., Sénési, S., Decharme, B., Alias, A., Chevallier, M., et al. (2019). Evaluation of CMIP6 DECK experiments with CNRM-CM6-1. *Journal of Advances in Modeling Earth Systems*, *11*(7), 2177–2213. https://doi.org/10.1029/2019MS001683
Wang, B., Wu, R. G., & Fu, X. H. (2000). Pacific-East Asian teleconnection: How does ENSO affect East Asian climate? *Journal of Climate*, *13*(9), 1517–1536. https://doi.org/10.1175/1520-0442(2000)013<1517:peathd>2.0.co;2
Wang, B. S., Goodkin, N. F., Angeline, N., Switzer, A. D., You, C. F., & Hughen, K. (2011). Temporal distributions of anthropogenic Al, Zn and Pb in Hong Kong Porites coral during the last two centuries. *Marine Pollution Bulletin*, *63*(5–12), 508–515. https://doi.org/10.1016/j.marpolbul.2011.02.011
Wang, G., Chen, D., & Su, J. (2006). Generation and life cycle of the dipole in the South China Sea summer circulation. *Journal of Geophysical Research*, *111*(C6). https://doi.org/10.1029/2005JC003314
Wang, L., Chen, W., & Huang, R. H. (2008). Interdecadal modulation of PDO on the impact of ENSO on the East Asian winter monsoon. *Geophysical Research Letters*, *35*(20), 4. https://doi.org/10.1029/2008gl035287
Watanabe, T., Winter, A., & Oba, T. (2001). Seasonal changes in sea surface temperature and salinity during the Little Ice Age in the Caribbean Sea deduced from Mg/Ca and $^{18}O/^{16}O$ ratios in corals. *Marine Geology*, *173*, 21–35. https://doi.org/10.1016/s0025-3227(00)00166-3
Weber, J. N. (1973). Incorporation of Strontium into reef coral skeletal carbonate. *Geochimica et Cosmochimica Acta*, *37*(9), 2173–2190. https://doi.org/10.1016/0016-7037(73)90015-x
Webster, P. J., & Lukas, R. (1992). TOGA COARE—The Coupled Ocean Atmosphere Response Experiment. *Bulletin of the American Meteorological Society*, *73*(9), 1377–1416. https://doi.org/10.1175/1520-0477(1992)073<1377:tctcor>2.0.co;2
Williams, K. D., Copsey, D., Blockley, E. W., Bodas-Salcedo, A., Calvert, D., Comer, R., et al. (2018). The Met Office Global Coupled Model 3.0 and 3.1 (GC3.0 and GC3.1) configurations. *Journal of Advances in Modeling Earth Systems*, *10*(2), 357–380. https://doi.org/10.1002/2017MS001115
Wu, B., Zhou, T., & Li, T. (2009). Seasonally evolving dominant interannual variability modes of East Asian climate. *Journal of Climate*, *22*, 2992–3005. https://doi.org/10.1175/2008jcli2710.1
Wu, B. Y., & Wang, J. (2002). Winter Arctic Oscillation, Siberian High and East Asian winter monsoon. *Geophysical Research Letters*, *29*(19), 1–4. https://doi.org/10.1029/2002gl015373
Xie, S.-P., Hu, K., Hafner, J., Tokinaga, H., Du, Y., Huang, G., & Sampe, T. (2009). Indian Ocean capacitor effect on Indo-Western Pacific climate during the summer following El Nino. *Journal of Climate*, *22*, 730–747. https://doi.org/10.1175/2008jcli2544.1
Xu, M., Chang, C. P., Fu, C. B., Qi, Y., Robock, A., Robinson, D., & Zhang, H. M. (2006). Steady decline of East Asian monsoon winds, 1969–2000: Evidence from direct ground measurements of wind speed. *Journal of Geophysical Research*, *111*(D24), 8. https://doi.org/10.1029/2006jd007337
Yan, H., Wei, W., Soon, W., An, Z., Zhou, W., Liu, Z., et al. (2015). Dynamics of the intertropical convergence zone over the western Pacific during the Little Ice Age. *Nature Geoscience*, *8*(4), 315–320. https://doi.org/10.1038/ngeo2375
Yan, X. H., Ho, C. R., Zheng, Q., & Klemas, V. (1992). Temperature and Size Variabilities of the Western Pacific Warm Pool. *Science*, *258*(5088), 1643–1645. https://doi.org/10.1126/science.258.5088.1643